Title

MEASUREMENT OF REFRACTIVE INDICES AND STUDY OF ISOTROPIC-NEMATIC PHASE TRANSITION BY THE SURFACE PLASMON TECHNIQUE

Author

Chu, K.C.

Publication Date

1979-07-01

Lawrence Berkeley Laboratory
UNIVERSITY OF CALIFORNIA, BERKELEY, CA

Materials & Molecular Research Division

Submitted to Molecular Crystals and Liquid Crystals

MEASUREMENT OF REFRACTIVE INDICES AND STUDY OF ISOTROPIC-NEMATIC PHASE TRANSITION BY THE SURFACE PLASMON TECHNIQUE

K. C. Chu, C. K. Chen, and Y. R. Shen

July 1979

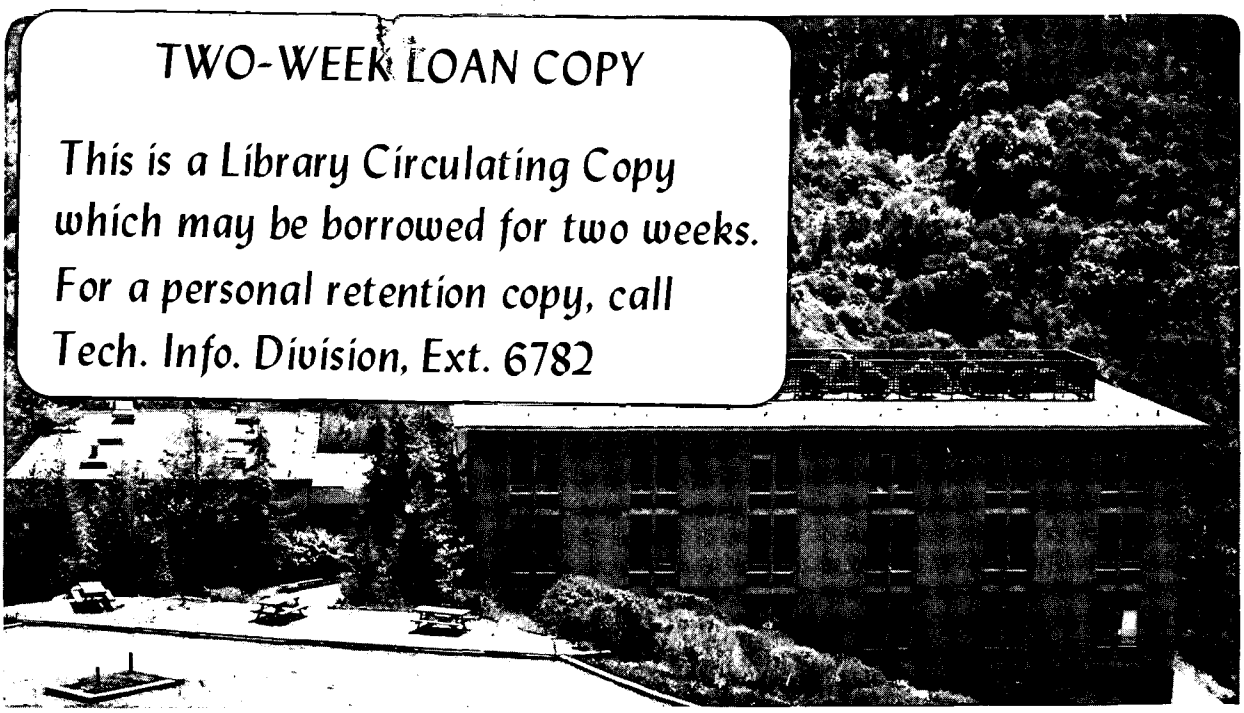

Prepared for the U. S. Department of Energy
under Contract W-7405-ENG-48

DISCLAIMER

Submitted to Mol. Cryst. Liq. Cryst. LBL-9398

MEASUREMENT OF REFRACTIVE INDICES AND STUDY OF ISOTROPIC-NEMATIC PHASE TRANSITION BY THE SURFACE PLASMON TECHNIQUE

K. C. Chu and C. K. Chen

Materials and Molecular Research Division
Lawrence Berkeley Laboratory
University of California, Berkeley, California 94720

Y. R. Shen

Department of Physics
University of California, Berkeley, California 94720

JULY 1979

ABSTRACT

The surface plasmon technique is employed to measure the refractive indices and to probe the nematic-isotropic phase transition of 4-cyano-4'-n-pentylbiphenyl. Coexistence of isotropic and nematic phases in a 60 mK range and a hysteresis effect of the phase transition have been observed. A diffuse droplet model is used to estimate the supercooling and superheating range.

I. Introduction

In recent years, surface plasmons have attracted much attention because of their potential applications in material studies.[1] These waves are electromagnetic waves propagating along the interface between a metal and a dielectric. The propagation characteristics depend critically on the bulk properties of the metal and the dielectric. Therefore, surface plasmon waves can be used to probe the optical constants of the boundary media.[2] However, since the surface waves are physically confined to a very narrow region around the interface, their propagation characteristics are also quite sensitive to the surface conditions of the media. Thus, they can be used to study adsorbed molecules[3] and overlayers[4] on metal surfaces.

In this work, we show that we can use the surface plasmon technique to measure the refractive indices of liquid crystals with an accuracy better than 1×10^{-3}. We have measured the refractive indices of the liquid crystalline material 4-cyano-4'-pentylbiphenyl (PCB) as functions of temperature, in particular, in the region near the isotropic-nematic phase transition. Because of the high sensitivity of the technique, we were able to probe the phase transition in great detail. We have found coexistence of the two phases, a hysteresis effect of the transtion, and supercooling and superheating in a temperature range of 60 mK around the nominal transition temperature. That surface phasmons can be used to probe phase transition was proposed earlier by Agranovich.[5] Our experiment here is the first demonstration of his idea.

Sections II and III give a brief account of the theory and the experimental arrangement, and Sec. IV describes the experimental results. Final-

ly, in Sec. V, the results in the phase transition region are discussed in terms of a diffused droplet nucleation model.

II. Theory

Two linear optical methods are generally used to excite surface plasmons on a metal-dielectric interface. The Otto method[6] uses a prism (or grating) on top of the metal surface, and the Kretschman[2] method uses an evaporated metal film on a prism. We have adopted the Kretschman method in our experiment as shown in Fig. 1. The laser beam with a TM polarization is directed onto the metal film through the prism side and the reflected beam is measured. Let the normal to the interface be along $\hat{z}$ and the plane of incidence in $\hat{x} - \hat{z}$. The reflectivity is given by

$$R(\theta) = \left| \frac{r_{12} + r_{23}\exp(i2k_{2z}d)}{1 + r_{12}r_{23}\exp(i2k_{2z}d)} \right|^2 . \qquad (1)$$

Here, the subindices 1, 2, and 3 refer to prism, metal, and liquid crystal respectively, θ is the angle of incidence at the metal film in the prism, d is the thickness of the metal film, k_{2z} is the complex z-component of the light wavevector in the metal, $k_{2z} = [(\omega/c)^2 n_2^2 - k_x^2]^{1/2}$, $k_x = k \sin\theta$ is the real x-component of the wavevector, r_{12} and r_{23} are the Fresnel reflection coefficients at the prism-metal and metal-liquid boundaries respectively.

$$r_{12} = (n_2^2 k_{1z} - n_1^2 k_{2z})/(n_2^2 k_{1z} + n_1^2 k_{2z})$$

$$r_{23} = (n_{3x}^2 k_{2z} - n_2^2 k_{3z})/(n_{3x}^2 k_{2z} + n_2^2 k_{3z}) \qquad (2)$$

$$k_{1z} = [(\omega/c)^2 n_1^2 - k_x^2]^{1/2}$$

$$k_{3z} = [(\omega/c)^2 n_{3z}^2 - k_x^2]^{1/2} \times (n_{3x}/n_{3z})$$

where n's are the refractive indices of the media. We have $n_{3x} = n_{3z} = n_\perp$ if the director $\hat{n}$ of the liquid crystal is aligned parallel to $\hat{y}$, and $n_{3x} = n_\perp$ and $n_{3z} = n_\parallel$ if $\hat{n}$ is aligned parallel to $\hat{z}$. With the liquid crystal in the isotropic phase, we have $n_{3x} = n_{3z} \equiv n_3$.

As θ increases above the critical angle

$$\theta_c = \sin^{-1}(n_{3x}/n_2) \tag{3}$$

the incoming beam is totally reflected, but then when θ reaches a value approximately satisfying the dispersion relation of the surface plasmon

$$1 + r_{12}r_{23}\exp(i2k_{2z}d) = 0, \tag{4}$$

the reflectivity $R(\theta)$ drops drastically. Physically, this happens because the surface plasmon wave is now strongly excited by the incoming light. The width of the reflectivity dip is determined by the damping coefficient of the surface plasmon. The entire reflectivity curve is fully described by Eq. (1) if the optical constants of the media are known. Conversely, from the reflectivity curve, we can determine the optical constants of the media. In the present experiment, we use the latter procedure to find the refractive indices of the liquid crystalline medium.

III. Experimental Arrangement

As shown in Fig. 1, the sample assembly was composed of a high refractive index glass prism (Schott glass SF 57 with n = 1.8117), an evaporated film (~ 450 Å) of gold, and a ~ 100-μm layer of liquid crystal sandwiched between the gold film and a glass plate. In the nematic phase, the liquid crystal was aligned along either $\hat{y}$ or $\hat{z}$ by the usual surfactant method.[7] The liquid crystal we have studied is PCB. The material was purchased from BDH Inc., and used without further purification.

The sample assembly sat in a two-stage oven with temperature control. The temperature stability was better than 1 mK during a 15-minute scan of the reflectivity curve. The sample oven was then mounted on a rotating stage driven by a stepping motor. The rotation was controlled by a Tektronix 4051 minicomputer. The light source used for the reflectivity measurement was a cw Nd:YAG laser at 1.06 μm with its power attenuated to below 20 μw in order to avoid heating of the sample. The reflected beam was monitored by a silicon photodiode rotating at twice the angular speed of the sample cell. The measured intensity of the reflected beam was normalized against the incident beam intensity to yield reflectivity. It was then digitized and recorded by the minicomputer as a function of the angular position of the sample cell. Equation (1) was finally used to fit the reflectivity curve to deduce a value of the refractive index for the liquid crystal.

IV. Experimental Results

Typical reflectivity curves at $T < T_c$ and $T > T_c$ are shown in Figs. 2(a) and 2(c) respectively, where T_c is the isotropic-nematic transition

temperature. The solid curves on the figures were calculated from Eq. (1) by a nonlinear least-square fit program using the refractive index of the liquid crystal as a parameter to be deduced. The values of the optical constants and thickness of the gold film, required in the calculation, were on the other hand derived from a reflectivity curve in the isotropic phase, knowing the value of the refractive index of the liquid crystal from a separate critical angle measurement.

In the nematic phase, the liquid crystal has two refractive index components: $n_\perp$ and $n_\parallel$ respectively perpendicular and parallel to the direction of alignment $\hat{n}$. We deduced $n_\perp$ first from the measurements with $\hat{n}$ along $\hat{y}$ and then $n_\parallel$ from the measurements with $\hat{n}$ along $\hat{z}$. The results are shown in Table 1 and Fig. 3. The accuracy of these n values is $\lesssim 1 \times 10^{-3}$, and was limited by the angular resolution of our apparatus. As a check on the results, we conducted separate measurements of $n_\perp$ and $n_\parallel$ with the critical-angle method.[8] The results are also shown in Table 1 and Fig. 3. They match very well with the results deduced from the surface plasmon experiment.

The fit to the reflectivity curve should in principle yield both the real and imaginary parts of the refractive index. However, since the damping in the metal film is extremely large, the accuracy in determining the small imaginary part of the refractive index for the liquid crystal is very poor. We did notice a slight broadening of the reflectivity dip as the temperature decreases towards the isotropic→nematic transition, presumably because of the increasing scattering loss in the liquid crystalline medium.

The most interesting aspect of the surface plasmon technique is its

ability to probe the phase transition in detail. By raising or lowering the temperature of the sample in milli-degree steps, we found that there was a ~ 60 mK transition region where the isotropic and nematic phases coexist. Two reflectivity dips showed up in the region, as shown in Fig. 2(b); one corresponded to the nematic phase at ~ T_c and the other to the isotropic phase at ~ T_c. Their positions remained unchanged as the temperature varied, but their relative magnitude did change. As seen in Fig. 2(b), the double-dip reflectivity curve can be fit very well by the theoretical expression

$$R = xR_{Isotropic} + (1 - x)R_{Nematic} \qquad (5)$$

where x is the fraction of the medium in the isotropic phase, and $R_{Isotropic}$ and $R_{Nematic}$ are evaluated at ~ T_c. With decreasing temperature, the nematic dip grew in strength while the isotropic dip gradually disappeared, and vice-versa for increasing temperature. In Fig. 4, the results of how x varies with temperature in the transition region are shown with the temperature change in one direction and then the other. After each temperature change, the system was stabilized for 15 minutes and then the reflectivity curve was measured. Figure 4 shows that there is a clear hysteresis effect, characteristic of the first-order transition. We can define the mid-point of the hysteresis loop as the transition temperature T_c, and the width of the hysteresis loop as the supercooling-superheating range. We believe this is the first time such a hysteresis loop for the nematic-isotropic transition has ever been measured. In our experiment, the transition tmperature drifted slowly at a rate of $- 5.5 \times 10^{-4}$ K/hr. The

data points in the figure have been corrected for this transition temperature drift. A similar hysteresis loop has also been observed when we monitor the transparency of a He-Ne laser beam through a .5-cm liquid-crystal cell as a function of temperature in the phase-transition region.[9]

V. Discussion

The surface plasmon technique is sensitive to the surface characteristics. Therefore, care must be taken to achieve good surface alignment of the liquid crystal. An imperfect alignment will lead to a shift and broadening of the reflectivity curve. Surface condition of the metal film is also important in the determination of the refractive indices for the liquid crystal. In our experiment, we used the result at an isotropic temperature as a calibration point to deduce the optical constants and thickness of the gold film. One would think that the same information about the gold film could be derived from the reflectivity curve of the air-gold film-prism assembly. However, with air replacing the liquid crystal, the effective roughness of the film surface seen by the light is very different, and hence the effective optical constants deduced for the gold film will also be different. Thus, for calibration in the liquid crystal measurements, one must use a medium with approximately the same refractive index as the liquid crystal to find the effective optical constants of the gold film.

The observed phase transition spans over a range of about 60 mK, appreciably larger than the ~ 10 mK width of the hysteresis loop. This suggests that effects due to inhomogeneity must have prevailed in the observed transition. Different domains with different impurities or defect points

as nucleation centers could have different transition temperatures. The fraction x of the isotropic phase coexisting with the nematic phase then represented the size of the domains in the isotropic phase. One might think that surface irregularities on the gold film were the source of inhomogeneities causing this 60 mK spread in the transition temperature. However, we have observed a similar spread of the transition temperature in a bulk measurement, indicating that inhomogeneities probably existed throughout the bulk. Note that the size of each domain must be quite small since the diameter of our probe beam was only 1 mm. Our observation of the double dips favor the picture of domains instead of a transient layer of nematic phase on the metal surface because a uniform layer of nematic phase between the metal and the isotropic phase will only shift the position of the surface plasmon resonance.

Considering that each domain has its own transition temperature, the width of the hysteresis loop must then represent the supercooling-superheating range. Theoretically, we can use a diffused droplet model of nucleation to estimate the supercooling range.[10] We assume that the transition of a domain into the nematic phase starts from a nucleation center on the surface and expands in the form of a half spherical droplet. Below the transition temperature T_c' of the domain, the free energy (or Gibb's energy) of the nematic phase is smaller than that of the isotropic phase. So, the droplet tends to grow, but the positive surface energy between the isotropic and nematic interface opposes the growth. This results in supercooling. The actual transition will occur only when thermal fluctuation has created a nematic droplet larger than a critical size over which any expansion of the droplet leads to a net decrease in the free energy

of the system since the decrease of the volume energy then dominates over the surface energy.

We use the truncated series of the Landau-de Gennes free energy density expression

$$f(\vec{r}) = f_N(\vec{r}) + \frac{3}{4} L[\nabla S(\vec{r})]^2$$

$$f_N(\vec{r}) = f_o(T) + \frac{3}{4} a(T - T^*)S^2(\vec{r}) - \frac{1}{4} BS^3(\vec{r}) + \frac{9}{16} CS^4(\vec{r}) - - - \quad (6)$$

where f_o is the free energy density of the isotropic phase, S is the order parameter, and a, B, C, T^*, and L all have the usual meaning. We assume a half spherical nematic droplet of radius R with a uniform order parameter S(T) obtained by minimizing f_N with respect to S. The droplet is surrounded by a half spherical transition layer. To find the variation of the order parameter in the transition layer, we must minimize the total free energy of the system.

$$F = \frac{1}{2}\left(\frac{4}{3} \pi R^3\right) f_N(S(T)) + \frac{1}{2}\int_R^\infty 4\pi r^2 f(r) dr. \quad (7)$$

The minization leads to the Euler equation

$$\frac{d^2S}{dr^2} + \frac{2}{r}\frac{ds}{dr} - \frac{2}{3L}\frac{\partial f_N}{\partial S} = 0 \quad (8)$$

with the boundary conditions

$$S(R) = S(T) \text{ and } S(\infty) = 0.$$

To find S(r) from the above equation, we adopted numerical method by varying the slope $\partial S/\partial r$ at r = R and requiring $\partial S/\partial r \leq 0$ for $r \geq R$ with no discontinuity. A fourth-order Runge-Kutta method[11] was used in the calculation. After S(r) was found, the total free energy $\Phi(R)$ of forming the droplet from the isotropic phase was then calculated

$$\Phi(R) = \frac{1}{2}\left(\frac{4}{3}\pi R^3\right)(f_n(S(T)) - f_o) + \frac{1}{2}\int_R^\infty 4\pi r^2 (f(r) - f_o)dr. \qquad (9)$$

Thus by repeating the calculation with different R, a curve of Φ versus R at the given temperature could be plotted. Examples are shown in Fig. 5 for the liquid crystal PCB at three different temperatures. In the calculation, a = 0.087 J/cm^3K, B = 2.13 J/cm^3, and C = 1.73 J/cm^3 obtained by Coles[12] and L = 6×10^{-14} J/cm [13] were used. For each temperature below $T_c' = T^* + B^2/(27aC)$, the Φ versus R curve shows a maximum at $R = R^*$, indicating that R^* is a critical radius for the nematic droplet. If initially the droplet has a radius $R > R^*$, then it will keep growing until the entire domain is converted to the nematic phase. If initially $R < R^*$, then the droplet will shrink and disappear.

Suppose the initial droplet is created by thermal fluctuations. The probability of having a droplet with a radius R^* is given by

$$P(R^*) = \Phi(R^*)e^{-\Phi(R^*)/kT} \Big/ \int_o^{\Phi(R^*)} e^{-\Phi(R)/kT} d\Phi(R)$$

$$\simeq (\Phi(R^*)/kT)e^{-\Phi(R^*)/kT}. \qquad (10)$$

The nucleation rate J is the product of this probability and the rate Ω

of a droplet with about the critical radius being expanded beyond the critical size.

$$J = \Omega P(R^*). \tag{11}$$

This rate Ω should be approximately the inverse of the response time τ for expansion and shrinking of the droplet. We choose the response time of the fast shear mode[14] of the liquid crystal as τ. We then have

$$\Omega = 1/\tau \cong \eta q^2/\rho \tag{12}$$

where η is the shear viscosity coefficient, ρ is the density, and q is the wavevector of the mode. For PCB, $\eta \sim 0.1$ poise, $\rho \sim 1$ gm/cm^2, and q $\sim$ (thickness of the surface transition layer)$^{-1} \sim 5 \times 10^5$ cm^{-1}, we find $\Omega \sim 2.5 \times 10^{10}$ sec^{-1} and hence

$$J = 2.5 \times 10^{10}(\Phi(R^*)/kT)e^{-\Phi(R^*)/kT}\,\text{sec}^{-1}. \tag{13}$$

Consider a domain sitting at a temperature T for a time period t. If Jt = 1, then it means that the domain will definitely make an isotropic→nematic transition in t. We can define the temperatue at which this happens as the supercooling temperature T_{SC}. In our experiment, t = 1000 sec. Using Eq. (12), we obtain

$$\Phi(R^*, T_{SC})/kT_{SC} \simeq 34$$

$$T_c' - T_{SC} \simeq 25\ \text{mK}. \tag{14}$$

The above model for supercooling is admittedly rather crude and has much room for improvement, but it does predict a supercooling range of the order of magnitude as experimentally observed. A similar model can of course be used to estimate the superheating range, which is roughly the same as the supercooling range.

VI. Conclusion

The surface plasmon technique has been used to measure the refractive indices of the liquid crystal PCB. The accuracy can be better than 10^{-3}. It has also been used to probe the phase transition of PCB. Since the technique is not restricted by the strong scattering in the transition region, it can be used to monitor the detailed variation of the phase transition process. Coexistence of isotropic and nematic phases in a range of $\sim$ 60 mK around transition, together with a hysteresis effect upon heating and cooling, has been observed. A diffuse droplet model of nucleation can be used to give a correct order-of-magnitude estimate on the supercooling ahd superheating range.

Acknowledgement

K. C. C. and C. K. C. were supported by the Division of Materials Sciences, Office of Basic Energy Sciences, U. S. Department of Energy under contract No. W-7405-ENG-48 and Y. R. S. was supported by the NSF under Grant No. DMR78-18826. C. K. C. acknowledges partial support as an NSF Graduate Fellow from NSF Grant No. SMI76-12375.

References

1. G. Borstel and H. J. Falge, Appl. Phys. 16, 211 (1978).

2. E. Kretschmann, Zeit. Phys. 241, 313 (1971).

3. W. H. Weber, Phys. Rev. Lett. 39, 153 (1977).

4. J. G. Gordon II and J. D. Swalen, Opt. Comm. 22, 374 (1977).

5. V. M. Agranovich, JETP Lett. 24, 558 (1976).

6. A. Otto, Zeit. Phys. 216, 398 (1968).

7. F. J. Kahn, Appl. Phys. Lett. 22, 386 (1973).

8. D. Riviere, Y. Levy, and C. Imbert, Opt. Comm. 25, 206 (1978).

9. J. W. Cahn, J. Chem. Phys. 30, 1121 (1959).

10. T. Bischofberger, K. C. Chu, and Y. R. Shen, unpublished.

11. D. McCracken and W. S. Dorn, Numerical Methods and Fortran Programming (Wiley, New York, 1964).

12. H. J. Coles, Mol. Cryst. Liq. Cryst. 492, 67 (1978).

13. E. B. Priestley, P. J. Wojtowicz, and P. Sheng, editors, Introduction to Liquid Crystals (Plenum, New York, 1975).

14. P. C. Martin, O. Parodi, and P. S. Pershan, Phys. Rev. A6, 2401 (1972).

Table 1 Refractive indices of 4-cyano-4'-n-pentylbiphenyl versus temperature (λ = 1.064 μ).

Temperature(°C)	$n_{\perp}$	$n_{\parallel}$	Method
23.09	1.516	1.683	a
24.2	1.516	1.681	b
25.71	1.517	1.677	a
26.2	1.517	1.675	b
28.63	1.519	1.668	a,b
31.0	1.521	1.660	a,b
33.15	1.524	1.650	a
34.2	1.527	1.642	b
34.24	1.527	1.641	a
34.9	1.532	1.632	a,b
35.1	1.564		b
35.6	1.563		b
36.37	1.562		a,b
40.2	1.560		b
45.0	1.557		b

a critical angle method

b surface plasmon method

Figure Captions

Fig. 1 Sample cell with incoming and outgoing beams.

Fig. 2 Reflectivity versus the angle of incidence θ shown in Fig. 1. The solid curves are theoretical curves obtained by nonlinear least square fitting.

Fig. 3 Refractive indices of 4-cyano-4'-n-petylbiphenyl versus temperature.

- o obtained by the surface plasmon technique
- • obtained by the critical angle method

Fig. 4 Fraction of the isotropic phase as a function of temperature in the transition region. Heating and cooling exhibit the hysteresis effect.

Fig. 5 Free energy of the nematic droplet versus its radius. Here $\Delta T = T_c' - T$.

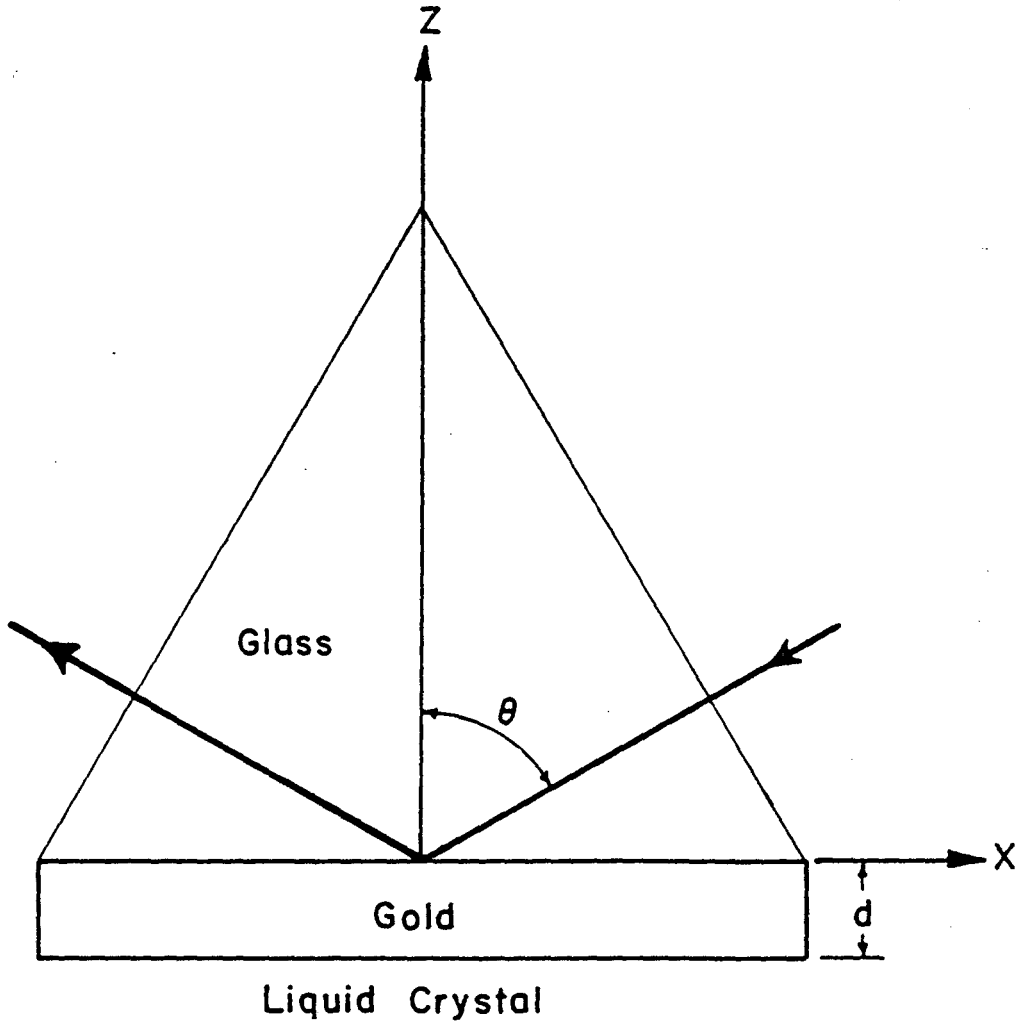

XBL797-6534

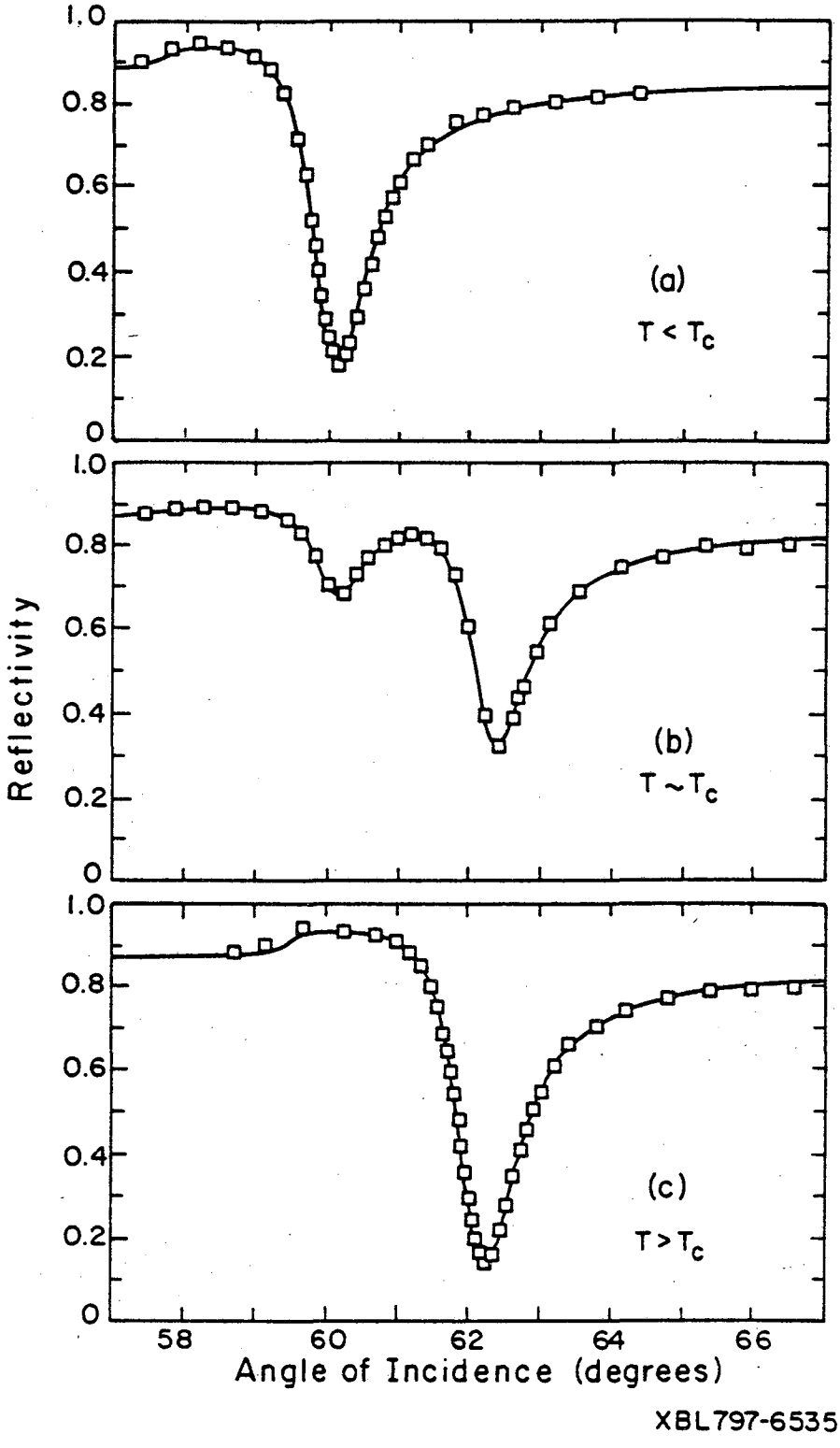
1.0
0.8
0.6
0.4
0.2
0
(a)
T < Tc
(b)
T ~ Tc
(c)
T > Tc
Reflectivity
58
60
62
64
66
Angle of Incidence (degrees)

XBL797-6535

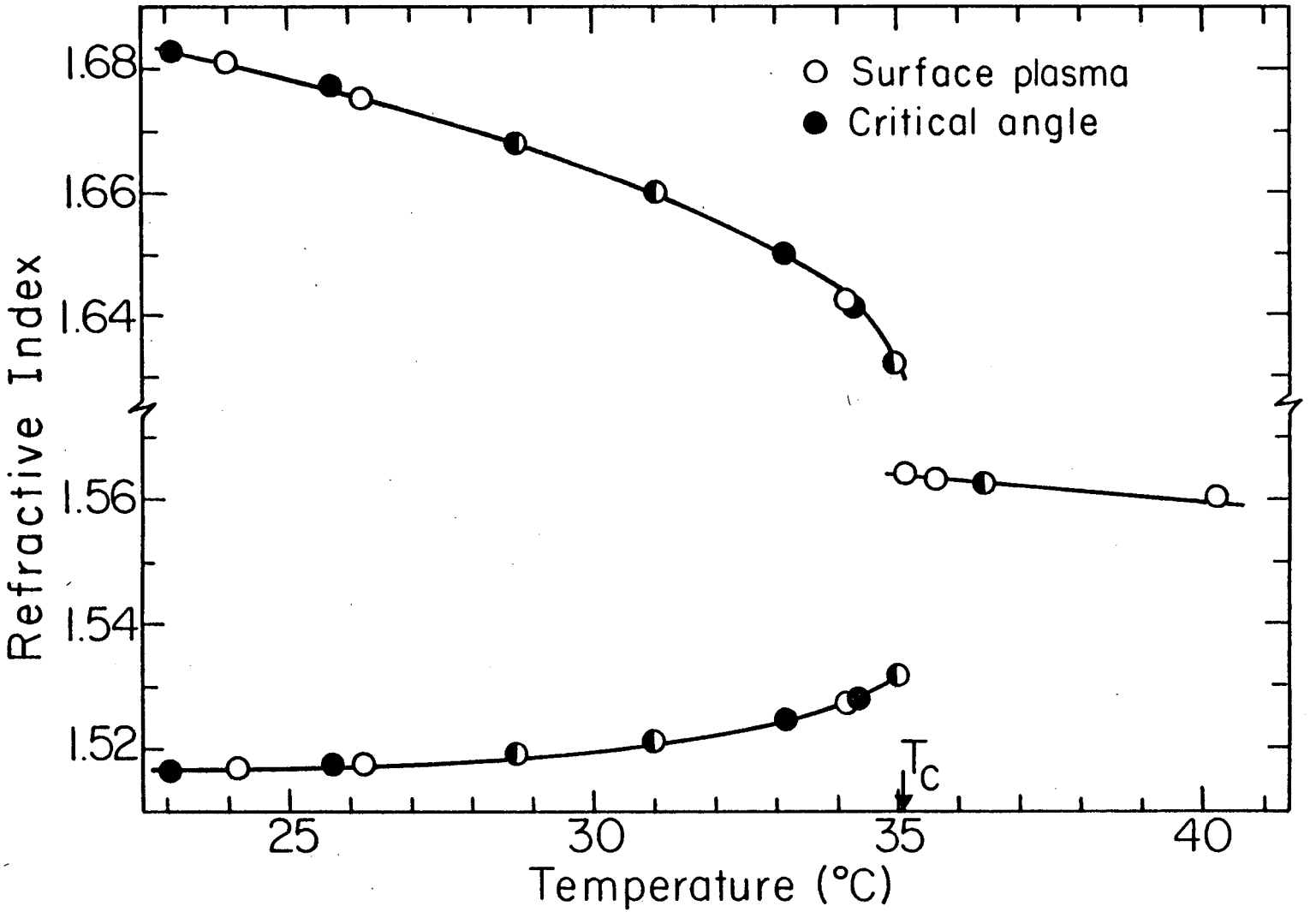
Surface plasma
Critical angle
Refractive Index
1.68
1.66
1.64
1.56
1.54
1.52
T_c
25
30
35
40
Temperature (°C)

XBL 797-6536

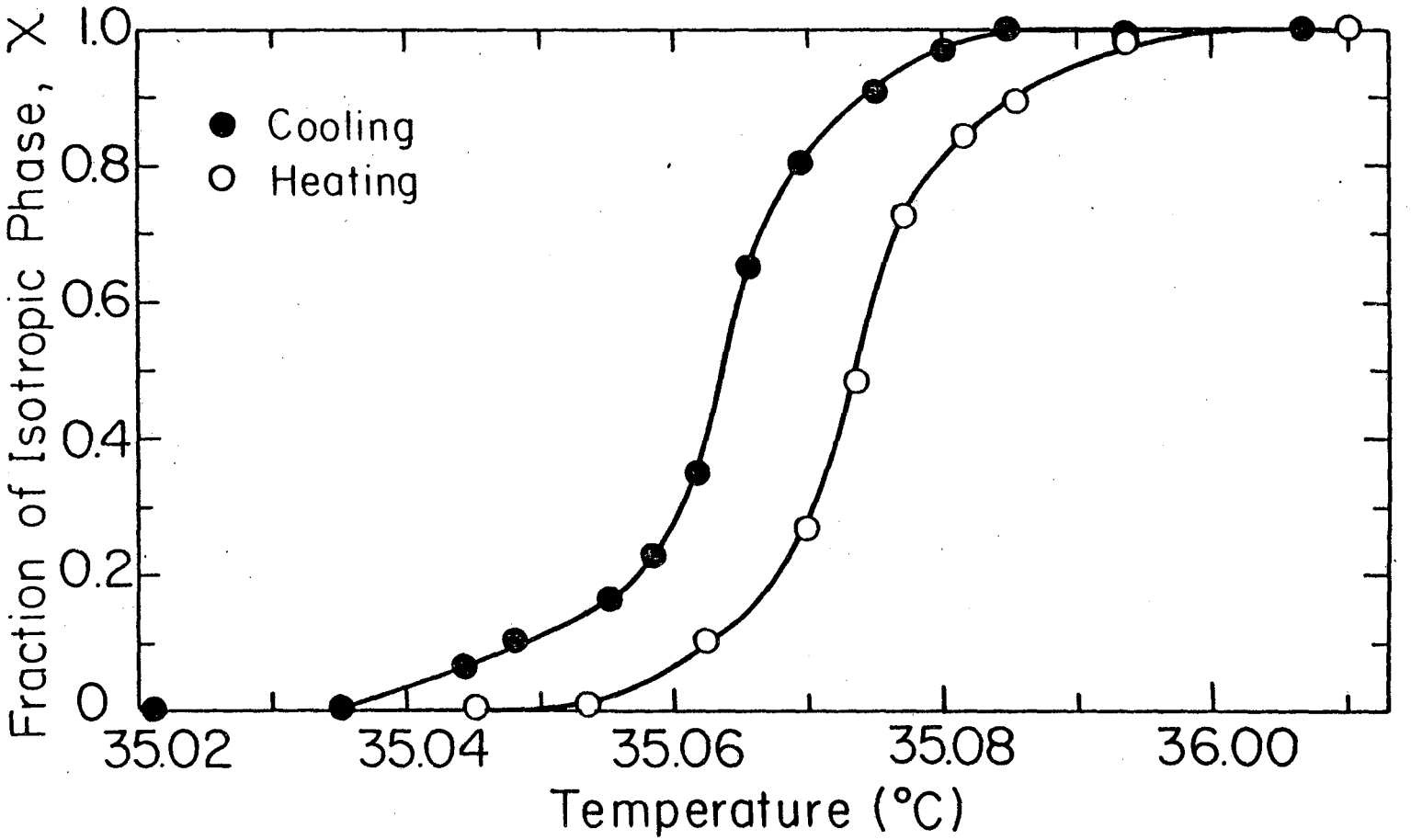
Fraction of Isotropic Phase, X
1.0
0.8
0.6
0.4
0.2
0
Cooling
Heating
35.02
35.04
35.06
35.08
36.00
Temperature (°C)

XBL 797-6537

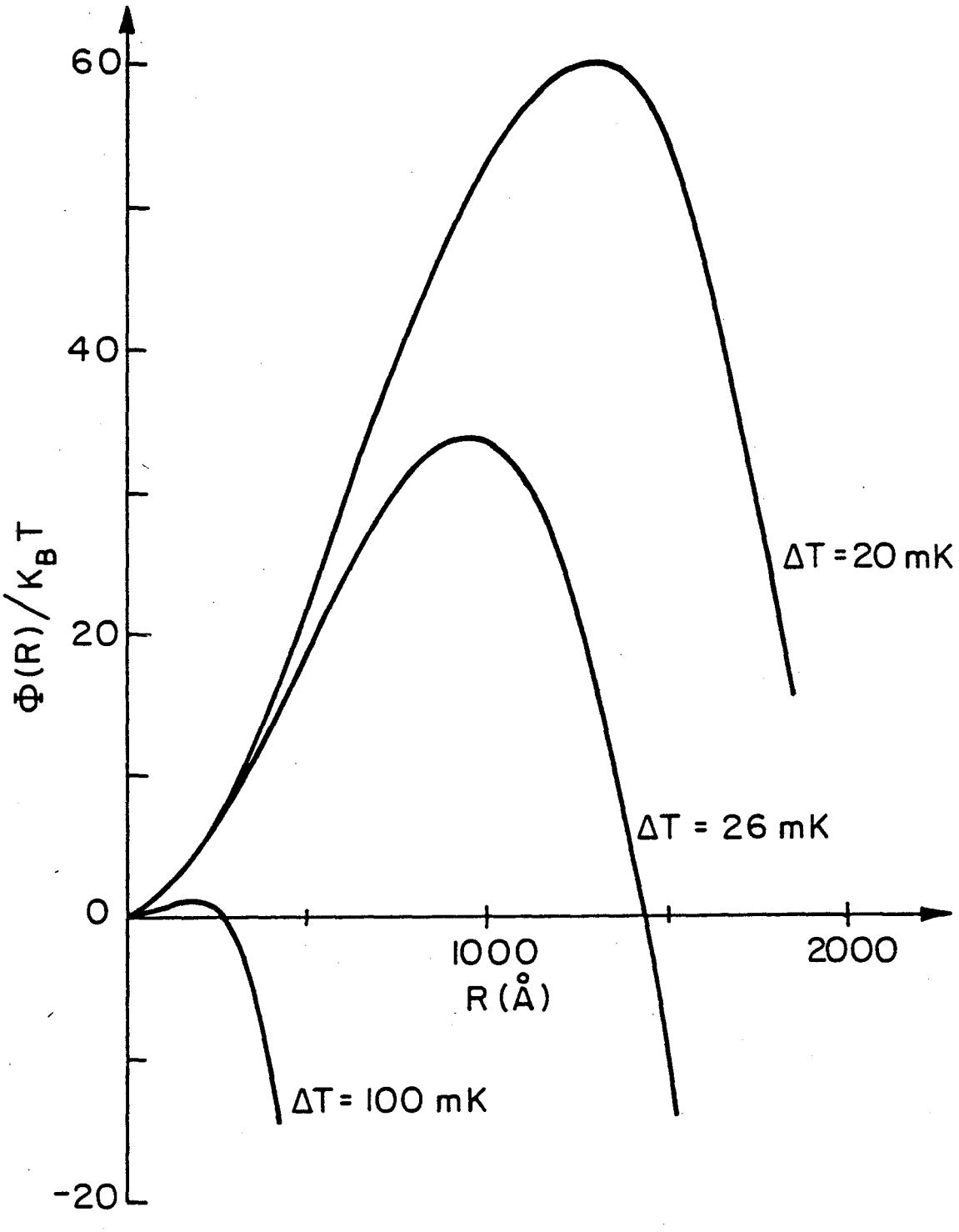

XBL 797-6538

This report was done with support from the Department of Energy. Any conclusions or opinions expressed in this report represent solely those of the author(s) and not necessarily those of The Regents of the University of California, the Lawrence Berkeley Laboratory or the Department of Energy.

Reference to a company or product name does not imply approval or recommendation of the product by the University of California or the U.S. Department of Energy to the exclusion of others that may be suitable.

TECHNICAL INFORMATION DEPARTMENT
LAWRENCE BERKELEY LABORATORY
UNIVERSITY OF CALIFORNIA
BERKELEY, CALIFORNIA 94720